polymers

MDPI

Article

Organic–Inorganic Double-Gel System Thermally Insulating and Hydrophobic Polyimide Aerogel

Liyao Xiong †, Weijie Zheng †, Shenglong Cao and Yuying Zheng *

College of Materials Science and Engineering, Fuzhou University, Fuzhou 350116, China; o5cookie@163.com (L.X.); 13290987197@163.com (W.Z.); csl239230@163.com (S.C.)
* Correspondence: yyzheng@fzu.edu.cn
† These authors contributed equally to this work.

Abstract: Aerogel materials are used in various fields, but there is a shortage of aerogel materials with an excellent combination of mechanical properties, thermal stability, and easy preparation. In this study, polyimide aerogel materials with superior mechanical properties, thermal stability, and low thermal conductivity were prepared by forming a double-gel system in the liquid phase. The amino-modified gel, prepared by coating SiO_2 nano-microspheres with GO through a modified sol-gel method (SiO_2@GO-NH_2), was subsequently homogeneously dispersed with PAA wet gel in water to form a double-gel system. The construction of a double-gel system enabled the PI aerogel to shape a unique honeycomb porous structure and a multi-layered interface of PI/SiO_2/GO. The final obtained PI aerogel possessed effective thermal conductivity (0.0309 W/m·K) and a high specific modulus (46.19 m^2/s^2). In addition, the high thermal stability (543.80 °C in Ar atmosphere) and the ability to retain properties under heat treatment proved its durability in high thermal environments. The hydrophobicity (131.55°) proves its resistance to water from the environment. The excellent performance of this PI aerogel and its durability in thermal working environments make it possible to be applied in varied industrial and research fields, such as construction and energy, where heat and thermal insulation are required.

Keywords: thermal insulation; hydrophobic; thermal stability; aerogel; polyimide

Citation: Xiong, L.; Zheng, W.; Cao, S.; Zheng, Y. Organic–Inorganic Double-Gel System Thermally Insulating and Hydrophobic Polyimide Aerogel. *Polymers* **2022**, *14*, 2818. https://doi.org/10.3390/polym14142818

Academic Editor: Maria Bercea

Received: 10 June 2022
Accepted: 6 July 2022
Published: 11 July 2022

1. Introduction

The overconsumption of energy is becoming a critical issue, based on engineering, environmental, and economic challenges in modern industries [1–3]. Pursuing a novel material with high performance and energy efficiency is a forefront research topic in terms of industrial applications [4–7]. Aerogel, as an impressive commercial energy material, plays a crucial role in the thermal insulation field due to its high strength and low density, which can be subdivided into inorganic and organic aerogels. Inorganic aerogels, especially silica-derived aerogels, have emerged as representatives of the heat insulation field because of their highlighted inherent textural properties, and, more importantly, unprecedented thermal stability and multifunctional use [8–13]. Despite the promising performance of inorganic aerogels, the obvious intrinsic drawbacks, such as hygroscopicity, brittleness, and lack of compressive modulus, inhibit their applications [14]. Compared with inorganic aerogels, organic aerogels, which have tunable structural properties, are not stable in thermal conditions [15–19]. Therefore, developing organic–inorganic aerogels is imperative to achieve the desired performance. Additionally, designing an effective combination strategy represents a critical first step in the establishment of a bridge between inorganic and organic aerogels [14,20,21].

Many strategies have been achieved in the development of high-strength bonding of organic–inorganic aerogels so far. The functional modification of aerogels by introducing nano-fillers has gained significant research attention [22–25]. In early studies,

Wang et al. [26] built blocks of cellulose nanofibers and ZrP/RGO nanosheets, which provided an aerogel with ultralow thermal conductivity (0.018 W/m·K) and high Young's modulus (194 kPa). Moreover, Zhu et al. [27] created a modified hydroxyapatite/chitosan composite aerogel with good mechanical properties and thermal insulation. Additionally, recent works have exhibited an appealing tendency to form a mutually cross-linked network structure by using a principal skeleton, e.g., silica [20], polyacrylonitrile [28], aramid nanofiber [29], and sodium alginate skeleton [30], etc. However, despite the great success of the strategies mentioned above, the industrial application practicability is still restricted due to the complexity of the process.

In recent years, many attempts have been made to achieve dehydration of wet gel, including regular drying, supercritical CO_2, and freeze-drying, etc. Among them, supercritical CO_2 is considered to be a better candidate in the conversion from wet gel to aerogel, which could deliver an excellent microscopic pore structure. In early studies, Zhang et al. [31] prepared impressive low-density (~0.2 g/cm^3) aerogels using supercritical drying. In parallel, Ana Iglesias-Mejuto and her co-workers [32] verified the compatibility of 3D printing and supercritical CO_2 drying in the field of aerogels. Despite their promising performance, poor mechanical properties, lack of thermal stability, and complex processes remain their fatal flaws [5]. Accordingly, there is an urgent demand for a modified method to address the aforementioned issues by producing better performance.

Herein, we introduce a "double-gel" method in which SiO_2@GO-NH_2 gels were conveniently and effectively constructed using the sol-gel method, and dispersed in an aqueous system to form a double-gel system with poly amic acid (PAA) organic wet gels. The aqueous system allowed the two phases to be uniformly dispersed and mixed, while the amino modification improved the compatibility between both gels. After freeze-drying and heat treatment, the wet gels turn into aerogels during PAA and transform into one of the most thermally stable polymeric materials known, polyimide (PI). The multilayered interfacial structure and the compatible dispersion of the two phases bring superior mechanical properties, thermal insulation, thermal stability, thermal durability, and hydrophobicity to aerogels.

2. Materials and Methods

2.1. Materials

4,4′-diaminodiphenyl ether (ODA), pyromellitic dianhydride (PMDA), tetraethyl orthosilicate (TEOS), ammonium hydroxide solution (25%), and N,N-dimethylacetamide (DMAc) were supplied by Shanghai Macklin Biochemical Co., Ltd. (Shanghai, China). Triethylamine (TEA) and (3-aminopropyl) triethoxysilane (3ATPES) were purchased from Aladdin Reagent Co., Ltd. (Shanghai, China). Ethanol, potassium permanganate, sulfuric acid (98%), and hydrochloric acid (36–38%) were purchased from Sinopharm Chemical Reagent Co., Ltd. (Shanghai, China). Flake graphite was provided by Shanghai Jingchun Reagent Co., Ltd. (Shanghai, China). All the reagents mentioned above were analytical grade, unless otherwise indicated.

2.2. Preparation of Amino-Modified SiO_2@GO (SiO_2@GO-NH_2) Wet Gel by Sol-Gel Method

Graphene oxide (GO) was prepared using a modified Hummers' method [33].

SiO_2@GO -NH_2 wet gels were prepared using the sol-gel method. Specifically, 25 mg of GO was added to 75 mL of 20 vol% TEOS ethanol solution, ultrasonically treated for 30 min, which ensured the system was well dispersed. Afterward, 10.5 mL of 0.1 M hydrochloric acid was added to acidify the system and was then ultrasonically treated for 5 min to fully hydrolyze the TEOS. A total of 4.5 mL of 10.79 wt.% 3ATPES ethanol solution was titrated slowly with slow mechanical stirring to gel the system and stirred for 24 h. The SiO_2@GO-NH_2 wet gel was then obtained.

2.3. Preparation of Polyamic Acid (PAA) Precursors and Wet Gel

Using an ice bath, 5.2630 g of ODA was dissolved in 55 mL of DMAc at 0 °C. After stirring for 5 min, 4.7369 g of PMDA was slowly added to the system in batches. The molar ratio of PMDA-to-ODA was 50:51 to control the length of polymer chains. The product was slowly poured into DI water at 0 °C and washed four times with DI water and freeze-dried at −65°C to obtain the PAA precursor. The ether bonding of ODA and the non-coplanar PAA chains make the PAA chains more soluble in the chosen solvent (water) and facilitate hydrogen bonding interactions with the inorganic doped material [34,35]. The PAA precursor was mixed with water and TEA in a mass ratio of 1:10:0.5 at room temperature and stirred at high speed for 30 min to obtain the PAA wet gel [36].

2.4. Preparation of Polyimide (PI) Aerogels

The SiO_2@GO-NH_2 wet gel was dispersed in 7.5 g of water by high-speed stirring and ultrasound. This was followed by continuous stirring in an ice bath at 0 °C using a slower stirring speed, while adding a total of 11.5 g of PAA wet gel in five batches. Stirring was continued for 4 h until the system was homogeneous. The obtained organic–inorganic dual system wet gels were poured into molds and frozen in a cold trap at −65 °C for 4 h, before being freeze-dried for 48 h. The molds were pre-cooled in the cold trap in advance, with the lowest cold trap temperature chosen to reduce the size of ice crystals in the gel system. The obtained aerogels were heat-treated at 80 °C for 30 min, 110 °C for 30 min, 195 °C for 120 min, and 290 °C for 60 min under nitrogen protection to obtain PI aerogels and numbered PI-1 (1 represents the addition of 1 g SiO_2@GO-NH_2). Similarly, a series of PI aerogels were prepared with different ratios of SiO_2@GO-NH_2 wet gels to study the effect of doping amount on the aerogel properties; the prepared PI aerogels were named PI-0, PI-0.5, PI-1.5, and PI-2. The PI aerogels used for mechanical and thermal property tests were prepared using specific molds. The diameter of the obtained PI aerogel was 35 ± 0.5 mm and the height was 10 ± 0.2 mm.

2.5. Characterization

The Nicolet 570 FTIR spectrometer (Thermo Fisher Scientific, Agawam, MA, USA) was used to obtain FTIR spectra of SiO_2@GO-NH_2. Microstructure pictures and EDX maps of freeze-dried SiO_2@GO-NH_2 wet gels and PI aerogels were taken with a SUPRA 55 thermal field emission scanning electron microscope (Carl Zeiss, Berlin, Germany) (SEM). ATR-FTIR spectra of PI aerogels were obtained with a Nicolet iS50 Fourier Transform Infrared Spectrometer (Thermo Fisher Scientific, MA, USA). XRD data of PI aerogels were provided by using an ULTIMA III X-ray diffractometer (Nippon Rigaku, Tokyo, Japan). The DXR2Xi Confocal Laser Raman Spectrometer (Thermo Fisher Scientific, MA, USA) provided Raman spectra of PI-0, PI-0.5, and PI-1.5 samples. The photoelectron spectra of PI-0 and PI-1.5 aerogels were measured using the ESCALAB 250 X-ray photoelectron spectrometer (Agawam, VG, USA). The ^{13}C NMR data of PI-1.5 aerogel were acquired using an AVANCE III 500 Nuclear Magnetic Resonance Spectrometer (Bruker, Fällanden, Switzerland). The stress–strain curves of the aerogel samples were obtained using an INSTRON-1185 (INSTRON, Norwood, MA, USA). The thermal conductivity of the aerogel samples was investigated using a DZDR-S thermal conductivity meter (Dazhan Mechatronics, Singapore). The infrared photographs of PI-0 and PI-1.5 placed on the heating stage were taken using a DS-2TPH10-3AUF infrared camera (HIKVISION, Hangzhou Hikvision Digital Technology Co., Ltd., Hangzhou, China). The thermogravimetric data of each group of PI aerogels were tested using a STA449C/6/G simultaneous thermal analyzer (NETZSCH, Westendstr, Germany). The water contact angle of each group of PI aerogel samples was measured with a SL200A/B dynamic/static contact angle meter (Shanghai Solon, Shanghai, China).

3. Results and Discussion

3.1. Amino-Modified SiO_2@GO (SiO_2@GO-NH_2) Wet Gel

The preparation process of SiO_2@GO-NH_2 wet gel is shown in Figure 1a. The SEM image in Figure 2b shows uniform accumulation of silica particles on the graphene sheets, indicating that the silica in the wet gel system is grown diffusively as nano-spheres with graphene as the base. FT-IR spectra of SiO_2@GO-NH_2 gels prepared by the above experimental scheme, and general SiO_2@GO gels with the replacement of 3APTES with ammonia, are shown in Figure 1c. The peaks of both spectra contain -OH (3400 cm^{-1}), C=C (1630 cm^{-1}), and C=O (1350 and 1230 cm^{-1}) from GO, Si-O-Si- (1090 cm^{-1}), SiO_2, and Si-O-C (1130 cm^{-1}), which represents the interaction between SiO_2 and GO. In addition to the peaks shared in SiO_2@GO-NH_2, -NH_2 (3260 cm^{-1}) and C-N (1220 cm^{-1}) are also present. Such data indicate that 3ATPES underwent hydrolysis and co-growth with SiO_2 nano-spheres during the sol-gel process in the alcohol–water system. This co-growth process also serves to amino-modify the silica nano-spheres by functionalization through 3APTES [37].

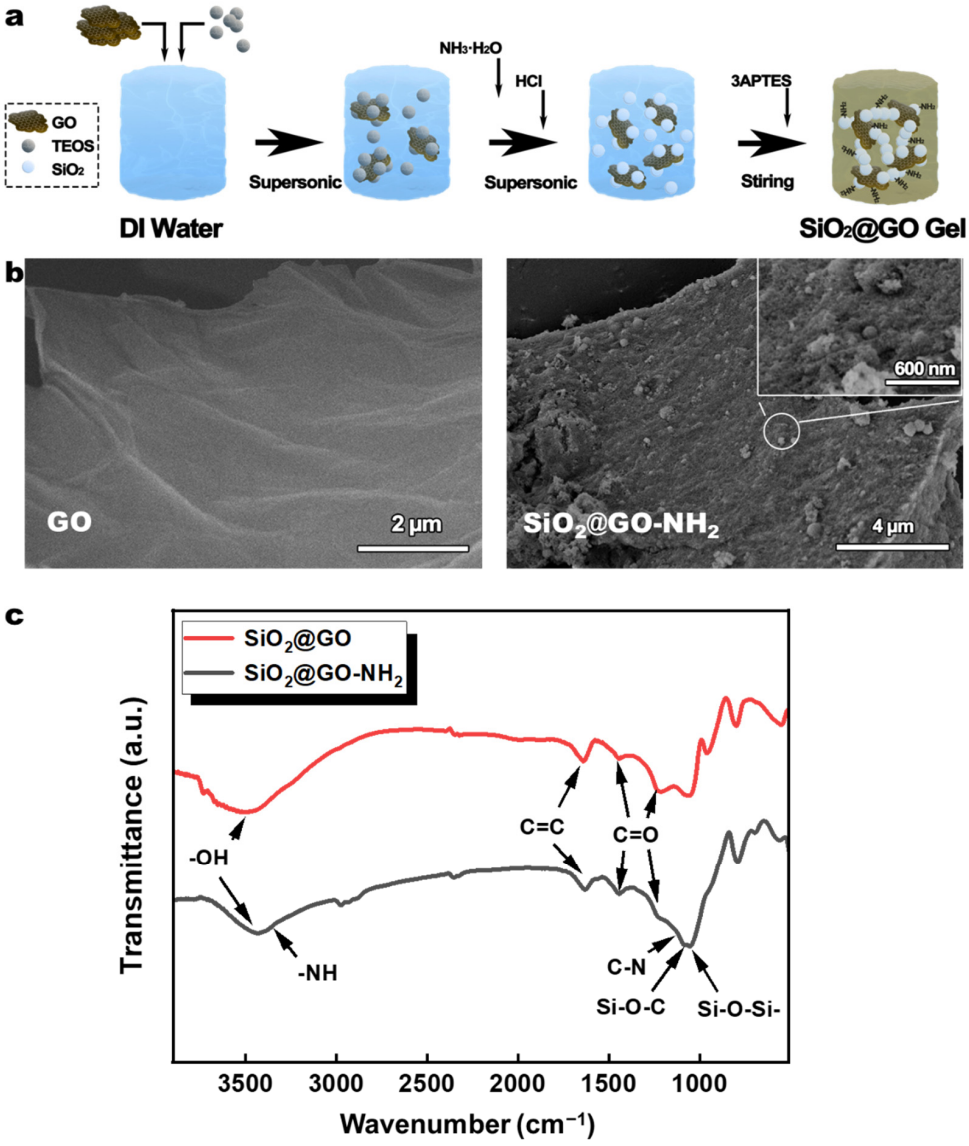

Figure 1. (**a**) Preparation process of SiO_2@GO-NH_2 wet gel. (**b**) SEM images of GO and SiO_2@GO-NH_2. (**c**) FT-IR spectra of SiO_2@GO and SiO_2@GO-NH_2.

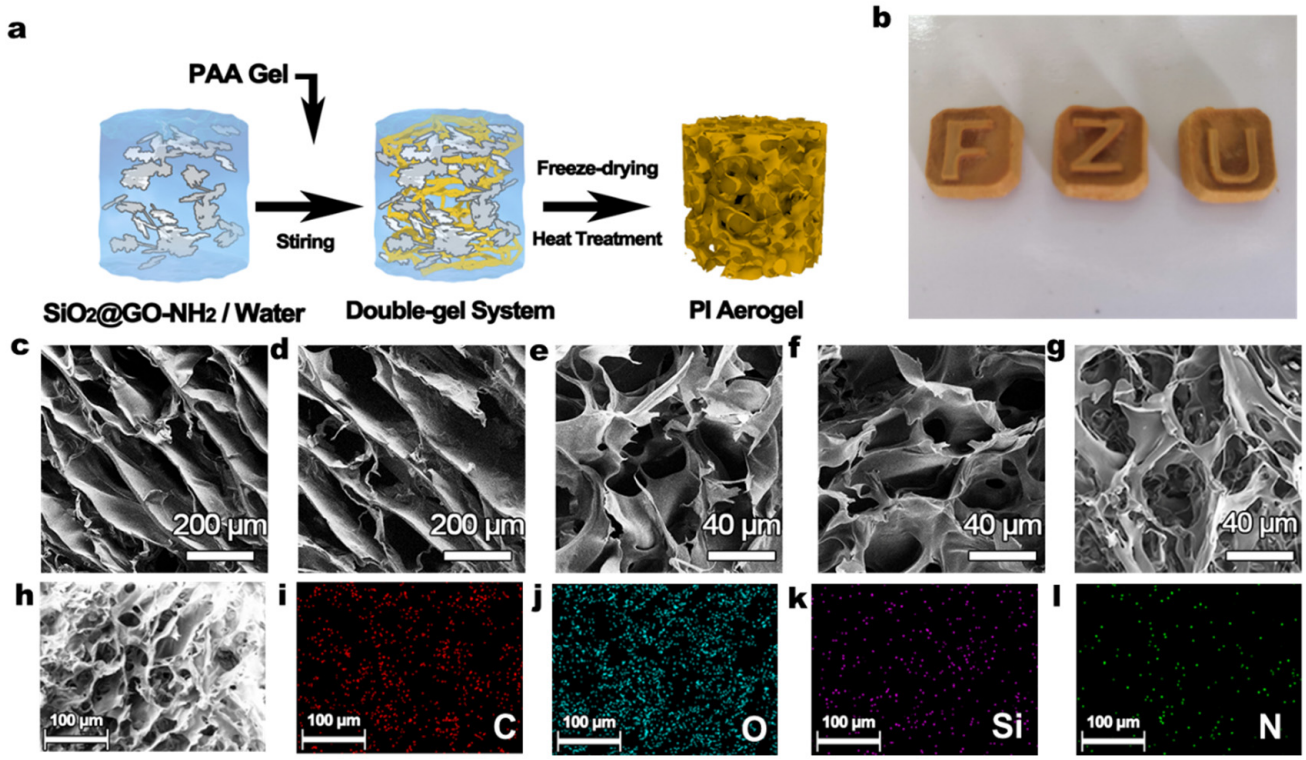

Figure 2. (**a**) Preparation process of double-gel PI aerogel. (**b**) A set of PI aerogels was prepared using custom molds, demonstrating the scalability of the preparation process. (**c**–**g**) SEM images of PI-0, PI-0.5, PI-1, PI-1.5, and PI-2. (**h**) Another SEM image and (**i**–**l**) EDS maps of PI-1.5 in the same area.

3.2. Preparation of PI Aerogel with Inorganic–Organic Double-Gel System

The preparation process of the PI aerogel is shown in Figure 2a. Specifically, this was to form a uniformly dispersed SiO_2@GO-NH_2 system from controlled quality SiO_2@GO-NH_2 gel in water, using high-speed stirring and ultrasonic treatment. Figure 2b shows the excellent processing properties of this aerogel preparation method, which can form finer and special structures with different molds. Figure 2c–h show typical SEM photographs of various PI aerogels. PI-1 to PI-2 formed a unique honeycomb, showing the limiting effect of the SiO_2@GO-NH_2 inorganic gel network on synergistic growth of the ice crystal/PAA linkage [38]. For comparison, PI-0 and PI-0.5 displayed a larger needle-like pore structure due to the spontaneous growth of polymer chains in the direction of the ice crystal growth edge during the freezing process. Typically, SiO_2@GO-NH_2 wet gel introduced in the PI-0.5 system is not enough to form an inorganic gel network, making the microstructure more similar to that of PI-0. The large pore size exhibited in PI-0 and PI-0.5 proves the difficulty of controlling the microscopic scale of polyimide aerogels prepared using the general freeze-drying method. In particular, the pores of PI-2 showed a lot of merging and fragmentation. The abnormal properties of PI-2 might be caused by the excessive addition of SiO_2@GO-NH_2 providing an overdone limiting effect, making it more difficult to form a stable honeycomb structure [39].

The elemental distribution on the microscopic scale of PI-1.5 was measured and analyzed using EDS. The results showed uniformity of the elements, while the microstructure of the original aerogel can still be observed in the images of each element, especially Si. The results observed by EDS demonstrate the homogeneity of the double-gel system, which means that the PI and the SiO_2@GO-NH_2 form the aerogel honeycomb structure on the nanoscale together.

3.3. Chemical Structure of PI Aerogel

The ATR-FTIR infrared spectra of the aerogel materials are shown in Figure 3a. The strong characteristic peaks at 1774 and 1710 cm^{-1} occurring on all spectra are attributed to the symmetric and asymmetric stretching of the C=O group of the imide double bond. The peak at 1375 cm^{-1} is attributed to the C-N stretching vibration, and a C=C stretching vibration at 1495 cm^{-1} was also observed. It can be concluded that the doping of SiO_2@GO-NH_2 and the double-gel network structure do not affect the chemical process of PI formation by imidization of PAA [40,41]. Figure 3b shows typical XRD data for each PI aerogel. All PI aerogels display characteristic polyimide amorphous structure peaks, but PI-0 and PI-0.5 have higher peak heights compared to other samples, which is related to the oriented structure formed during the aerogel and preparation process [42]. This also proves that the introduction of the SiO_2@GO-NH_2 gel changes the overall structure of polyimide aerogels.

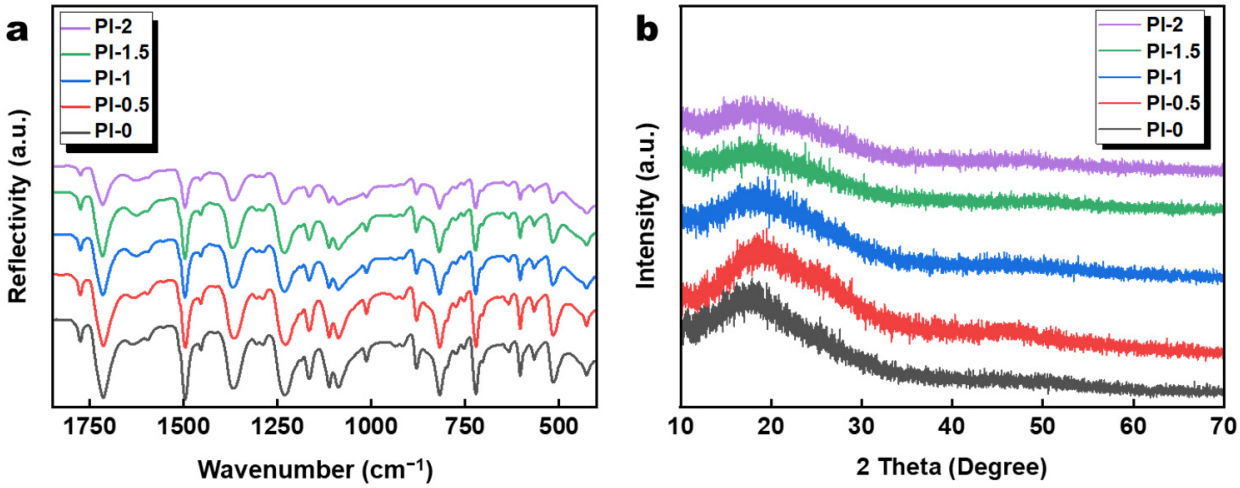

Figure 3. (**a**) FTIR-ATR spectra and (**b**) X-ray diffraction patterns of PI-0, PI-0.5, PI-1, PI-1.5, and PI-2.

Figure 4a shows the Raman spectra of PI-0, PI-0.5, and PI-1.5. All three spectra exhibited bright fluorescent signals, and the spectral bands around 1340 cm^{-1} can be attributed to the C-N stretching vibration, around 1590 cm^{-1} to the ring vibration of PI, and around 1740 cm^{-1} to the stretching vibration of C=O from PI and GO [43,44]. This may be caused by the convergence of the D-band of rGO (1330 cm^{-1}) and C-N stretching vibration (1340 cm^{-1}) with each other, the overlap of the G-band of rGO (1560 cm^{-1}) and the ring vibration of PI (1590 cm^{-1}), and the enhancement of the peak signal with an increase in the SiO_2@GO-NH_2 [45]. This evidence demonstrates the close association between PI chains and SiO_2@GO-NH_2 within aerogels.

To further verify the chemical bond structure and elemental composition of the aerogel material, XPS was used to analyze the PI-0 and PI-1.5 materials. The peaks of Si 2p can be deconvoluted into two groups of sub-bands, assigned to O-Si-O (102.9 eV) and O-Si-C (101.2 eV), representing the amino-modification by 3ATPES [37,46–48].

The solid-state ^{13}C NMR further reveals the chemical structure described by the previous characterizations. The peaks at 118, 123, and 136 ppm belong to graphene and aromatic carbon peaks on the PI chains [49]. The peak at 165 ppm belongs to the carbonyl carbon [50]. The peaks at 155 and 158 ppm, except for the observed double peaks, belong to aromatic carbon forming ether bonds on the PI chains, which are slightly shifted due to their chemical environment [51]. The peaks at 155 and 158 ppm belong to aromatic carbons forming ether bonds in the PI chains.

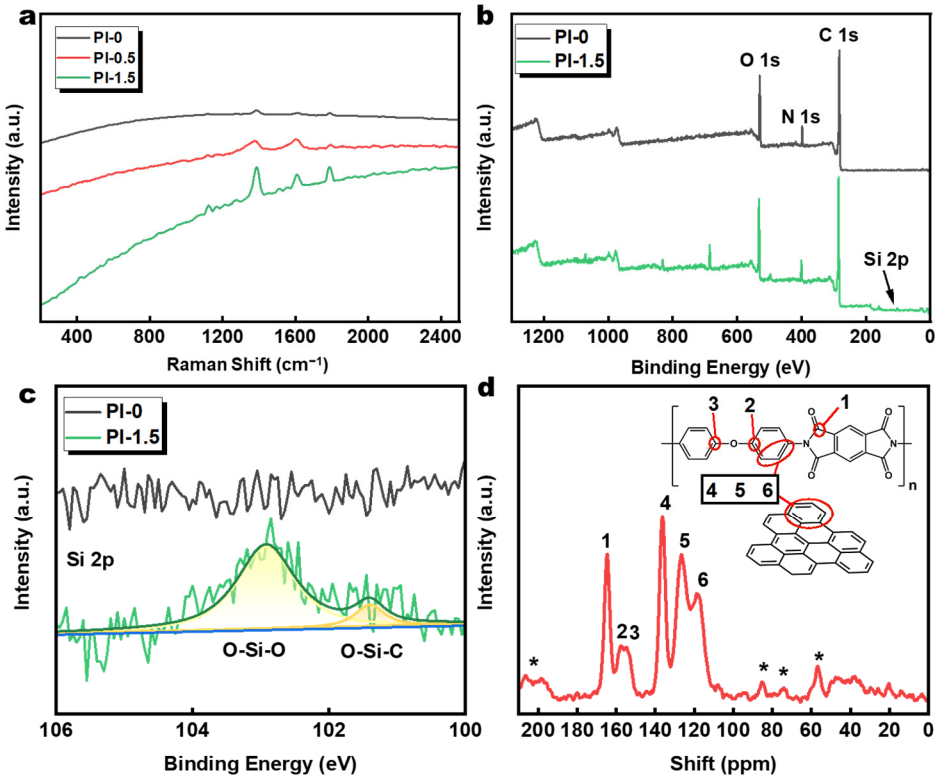

Figure 4. (**a**) Raman spectra of PI-0, PI-0.5, and PI-1.5. (**b**) XPS and (**c**) Si 2p spectra of PI-0 and PI-1.5. (**d**) Solid-state ^{13}C NMR spectra of the PI-1.5; * indicates peaks from spinning sidebands.

3.4. Properties of PI Aerogel

In practical applications, mechanical properties are often the key element in measuring the performance of aerogels. The densities of aerogels were acquired by averaging the results of three measurements of a 10 mm × 10 mm × 10 mm sized PI aerogel. In this way, we further obtained the specific moduli data of PI aerogels. Although it is generally believed that limited SiO_2 nanoparticles can improve the mechanical properties of polymeric materials to a certain extent, an excess can also lead to a decrease in mechanical properties [52,53]. This is because the addition of more SiO_2 leads to agglomeration of nanoparticles due to van der Waals forces and electrostatic adsorption, resulting in stress concentration between the SiO_2 and the polymer interface [54]. Although a large amount of SiO_2@GO-NH_2 was added into the system during the preparation of the PI aerogel in this study, the specific modulus of the original PI-1.5 sample still reached a relatively superior 46.19 m^2/s^2 while maintaining a low density (0.0441 g/cm^3). There are several reasons for this: (1) the high dispersion of SiO_2@GO-NH_2, (2) amino groups led to SiO_2@GO-NH_2 providing crosslinking sites and enhancing material compatibility, (3) the loading effect played by GO, and (4) the improvement in the structural properties of the given substrate by the silica-containing network [39,55]. As shown in Figure 5a, PI-0 and PI-0.5 samples have similar stress–strain curves, probably due to the similarity in microstructure. With the improvement in microstructure, the Young's moduli of the PI-1 and PI-1.5 samples are greatly enhanced. Interestingly, the two groups of aerogels are still maintained in the linear elastic region when strain exceeds 40%. Then, there is a sharp increase in the platform strain behavior and the densification state. This can be attributed to the energy dissipation effect of the cross honeycomb material and graphene with good toughness values [56]. However, the linear elastic region of PI-2 produces a certain decrease with damage to the microstructure and stress concentration, caused by excessive doping.

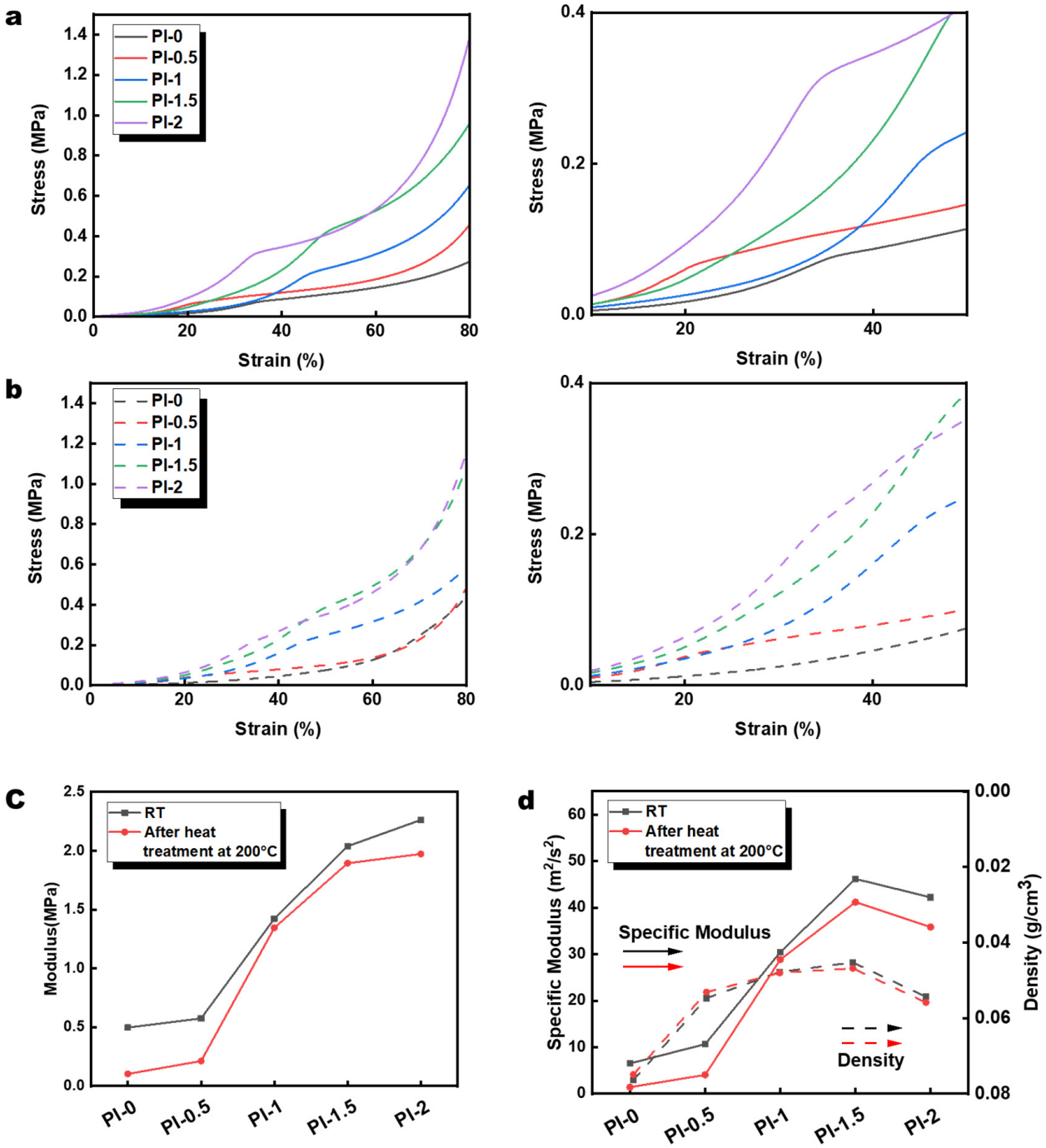

Figure 5. (**a**,**b**) The stress–strain curves, (**c**) Young's moduli, (**d**) specific moduli, and densities of PI-0, PI-0.5, PI-1, PI-1.5, and PI-2.

As a representative of heat-resistant polymers, PI aerogels should maintain good performance even after the influence of high temperatures. The PI aerogel was heat-treated at a constant temperature of 200 °C in the air for 24 h to investigate the property retention of PI aerogel after long-time heat treatment. The stress–strain curves of the heat-treated aerogels shown in Figure 5b, and the Young's moduli, specific moduli, and density data of the two sets of aerogels were statistically analyzed accordingly and are summarized in Figure 5c,d. It is not difficult to see that the moduli and specific moduli of polyimide aerogels decreased after heat treatment, created by the relaxation of internal stress and the destruction of the microstructure of polyimide aerogels after heat treatment [57]. However, PI-1.5 still

maintains a good Young's modulus (1.89 MPa) and specific modulus (41.21 m^2/s^2), which proves its durability and mechanical property retention under a long-term thermal environment. PI-1.5 produces huge mechanical property improvement compared with PI-1, based on the increase in filler content for polymeric materials, with constant microstructure and uniform dispersion of fillers [58]. Toughening is achieved. The Young's modulus of PI-2 (2.26 MPa) in PI aerogel preserved at room temperature without heat treatment improves compared with PI-1.5 (2.04 MPa). With an increase in density due to destruction of the microstructure ($\rho_{PI\text{-}2}$ = 0.0536 g/cm^3), the specific modulus of PI-2 (42.23 m^2/s^2) was shown to decrease. Instead, the Young's modulus of PI-1.5 and PI-2 (1.97 MPa) became closer after heat treatment. The stress–strain curves showed that the heat-treated PI-2 samples could also be maintained in the linear elastic region at more than 40% of the strain, further indicating the relaxation effect of heat treatment on the concentration of internal stress in the aerogel material.

Thermal insulation is an essential indicator of the energy efficiency of PI aerogels. The thermal resistance analysis of the aerogel material is exhibited in Figure 6. The PI-1.5 aerogel exhibited superior thermal resistance in the original state (0.0309 W/m·K) and after heat treatment (0.0328 W/m·K). The PI-1.5 aerogel exhibits competitive thermal conductivity in comparison with other similar PI aerogel/foam materials (Xue et al. 0.036 W/m·K [39], Zhang et al. 0.0311 W/m·K [51], and Jiang et al. 0.04106 W/m·K [59]). As shown in Figure 6a, the flowers placed on top of PI-1.5 showed no significant dehydration after 15 min of burning using an alcohol burner flame. The introduction of graphene generally leads to an increase in the thermal conductivity of the system, with the wrapping of graphene using SiO_2 preventing the formation of thermal pathways between graphene, thus eliminating its thermal conductivity [60,61]. The dispersion interval of the thermal resistance test data of the PI-0 sample has a larger error interval compared to that of the other samples, which may be due to the large pore size of the PI-0 sample. Unlike the similarity of mechanical properties, the thermal resistance of PI-0.5 (original: 0.0387 W/m·K; after heat treatment 0.0390 W/m·K) is much better than PI-0 (original: 0.0426 W/m·K; after heat treatment: 0.0425 W/m·K). The uniform dispersion of the inorganic gel phase in the aerogel system forms a PI/SiO_2/GO multilayer interface, which enhances the thermal resistance (Kapitza thermal resistance) [62]. The thermal resistance of PI-1 (original: 0.0332 W/m·K; after heat treatment: 0.0344 W/m·K) and PI-1.5 increased significantly compared to other aerogels, suggesting that the double-gel system improves the density and microscopic pore structure of the aerogel system. The increased content of SiO_2@GO-NH_2 enhanced the Kapitza thermal resistance of the system. As shown in Figure 6d, the infrared images of PI-0 and PI-1.5 are obtained by cutting the original aerogel samples into cylindrical test samples of 2 cm in height and 2 cm in diameter, and then placing them on a 200 °C heating stage for 60 min and photographing them using an infrared camera. PI-1.5 shows much slower thermal diffusion than PI-0, and the thermal resistance is consistent. The superior thermal and mechanical properties make the PI aerogel in this study a possible solution for construction, energy, and other applications [16].

The thermal properties of PI aerogels are discussed further by thermogravimetric analysis. The TGA data of PI aerogels were tested and analyzed, and are shown in Figure 7. PI-0 and PI-0.5 showed similar weight loss changes at 0–500 °C and the curves of both almost overlapped. The aerogel microstructure and other factors produce improvement with the addition of SiO_2@GO-NH_2, causing decreased weight loss rates of PI-1 and PI-1.5 at 0–500 °C compared to PI-0 and PI-0.5. The decomposition temperatures of PI-0, PI-0.5, PI-1, and PI-1.5 were 522.45, 539.30, 548.88, and 543.80 °C, respectively, when the weight loss reached 5% in the Ar atmosphere. While in the air, they were 384.03, 440.55, 457.22, and 496.03 °C. The improvement in thermal stability demonstrates the strong interaction between organic and inorganic components in the double-gel system [63]. In contrast, the weight loss rate and decomposition temperature (392.12 °C in Ar atmosphere and 248.35 °C in Air atmosphere) of the PI-2 aerogel at 0–500 °C produced a considerable

decrease, indicating that the excess SiO_2@GO-NH_2 for the disruption of the microstructure of the PI aerogel instead reduced the thermal stability of the aerogel [64].

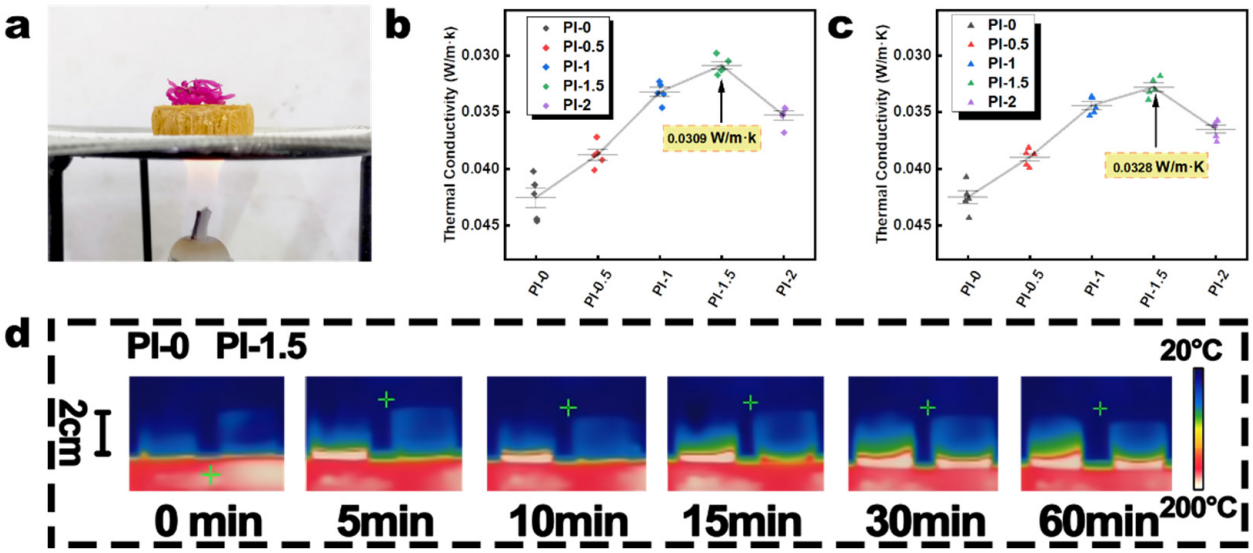

Figure 6. (**a**) PI-1.5 and flowers on the flame of the alcohol burner for 15 min. (**b**,**c**) Thermal conductivity of PI-0, PI-0.5, PI-1, PI-1.5, and PI-2 before and after heat treatment. (**d**) Infrared photo of PI-0 and PI-1.5 placed on a 200 °C heating stage for 60 min.

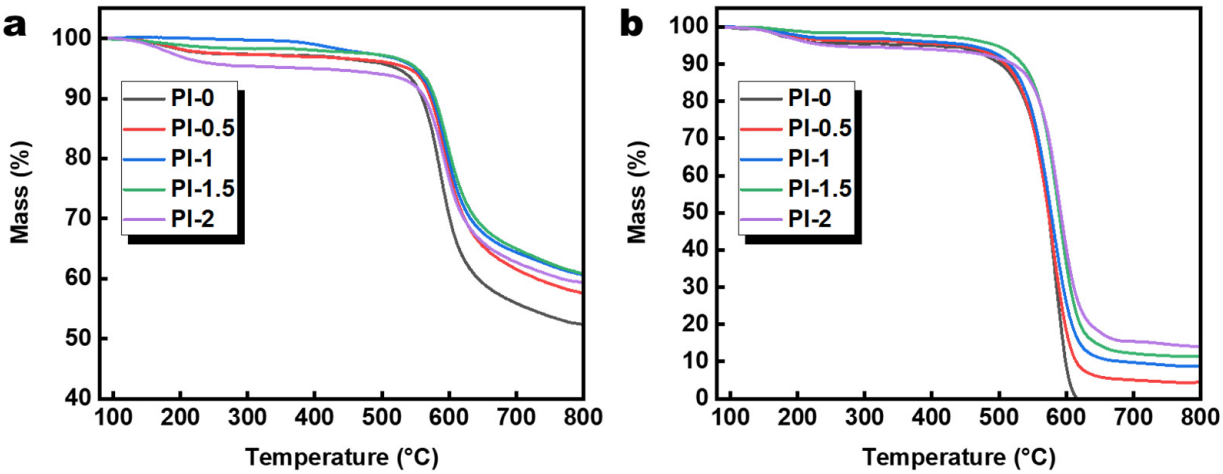

Figure 7. TGA curves of PI-0, PI-0.5, PI-1, PI-1.5, and PI-2 under (**a**) Ar and (**b**) air atmosphere.

If the PI aerogel can absorb moisture from the environment, the thermal insulation property could also reduce. As shown in Figure 8, the hydrophobicity of the PI aerogel was studied by measuring the water contact angle. Due to the capillarity caused by the poor microscopic structure of PI-0, the PI-0 aerogel absorbed all the tested droplets, indicating intrinsic hydrophilicity. The PI-0.5 sample had a water contact angle of 27.03°, indicating that the SiO_2@GO-NH_2 gel could provide the hydrophobicity of the PI aerogel. The water contact angle of PI-1 and PI-1.5 produced a tremendous leap. More specifically, the water contact angle of PI-1.5 reached 131.55°, which testifies to its high hydrophobicity. The controlled pore structure of aerogels allows an increase in surface roughness, thus improving the hydrophobicity of the aerogel surface. However, with heat treatment, the water contact angles of the PI aerogels all decreased. The increasing hydrophilicity can be attributed to the introduction of oxygen-containing functional groups or changes in the microstructure [12,65].

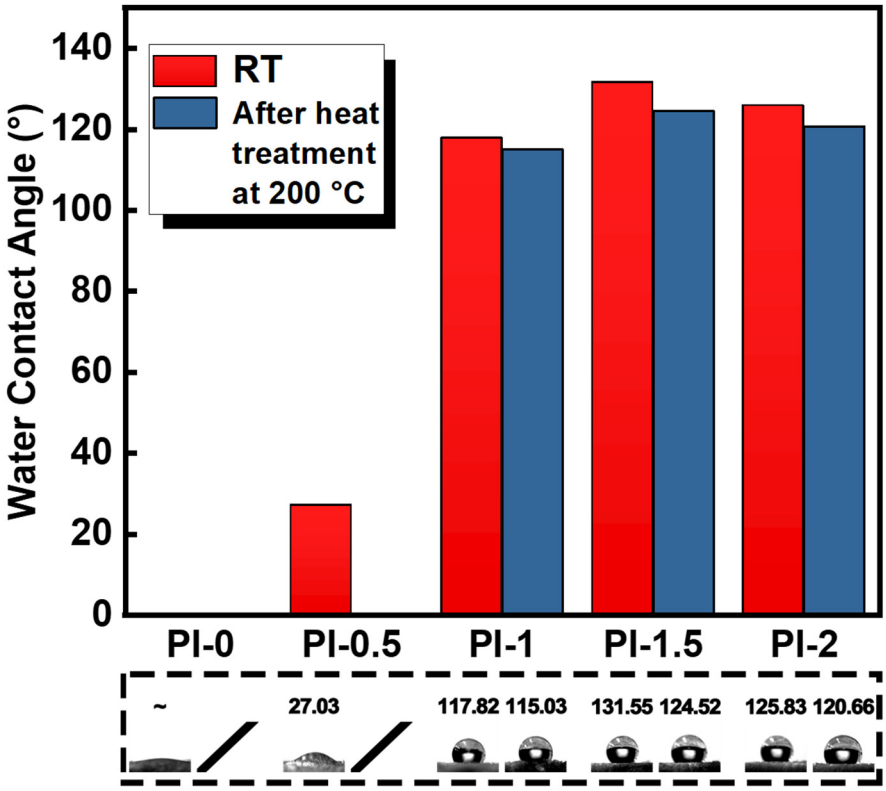

Figure 8. Contact angle data of PI-0, PI-0.5, PI-1, PI-1.5, and PI-2.

4. Conclusions

In summary, a double-gel system polyimide aerogel material was discussed in this study. A SiO_2@GO-NH_2 amino-modified wet gel was first fabricated via a novel sol-gel method, to obtain a SiO_2 uniformly coated GO material. Then, the PAA gel and SiO_2@GO-NH_2 gel were homogeneously dispersed under the liquid phase, to provide the double-gel system. After a series of subsequent treatments, the prepared PI aerogel had a microscopic porous honeycomb structure and multiple-layer interface, which provided good thermal resistance. The strong compatibility and binding of SiO_2@GO-NH_2 with PI also improved the low density (0.0442 g/cm^3), high specific modulus (46.19 m^2/s^2), effective thermal insulation properties (0.0309 W/m·K), high thermal stability (543.80 °C in Ar atmosphere), high hydrophobicity (131.55°), and ability to maintain performance after prolonged exposure to thermal environments. The performance improvement was due to the scientific introduction of SiO_2@GO-NH_2 and the construction of the double-gel system. The easy preparation process and superior performance make it suitable for wide applications within various industrial and research fields requiring thermal insulation.

Author Contributions: Conceptualization, L.X. and W.Z.; methodology, L.X. and W.Z.; software, L.X.; validation, L.X., W.Z. and S.C.; formal analysis, L.X. and W.Z.; investigation, L.X. and W.Z.; resources, L.X., W.Z. and S.C.; data curation, L.X., W.Z. and S.C.; writing—original draft preparation, L.X., W.Z., S.C. and Y.Z.; writing—review and editing, L.X., W.Z. and Y.Z.; visualization, L.X. and W.Z.; supervision, Y.Z.; project administration, Y.Z.; funding acquisition, Y.Z. All authors have read and agreed to the published version of the manuscript.

Funding: Financial support for this research from the University-Industry Cooperation Project of Fujian Province (2019H6012), Quanzhou City Science and Technology Program of China (2021C002R), Fujian Provincial Science and Technology Plan Project (2021H4004), and the Major Special Project of Fujian Province (2021HZ027002 & 2021HZ027021) is appreciated.

Institutional Review Board Statement: Not applicable.

Informed Consent Statement: Not applicable.

Data Availability Statement: Not applicable.

Acknowledgments: We thanks for the Financial support for this research from the University-Industry Cooperation Project of Fujian Province (2019H6012), Quanzhou City Science and Technology Program of China (2021C002R), Fujian Provincial Science and Technology Plan Project (2021H4004), and the Major Special Project of Fujian Province (2021HZ027002 & 2021HZ027021) is appreciated.

Conflicts of Interest: The authors declare no conflict of interest.

References

1. Memon, S.A. Phase change materials integrated in building walls: A state of the art review. Renew. *Sustain. Energy Rev.* **2014**, *31*, 870–906. [CrossRef]
2. Akeiber, H.; Nejat, P.; Majid, M.Z.A.; Wahid, M.A.; Jomehzadeh, F.; Famileh, I.Z.; Calautit, J.K.; Hughes, B.R.; Zaki, S.A. A review on phase change material (PCM) for sustainable passive cooling in building envelopes. *Renew. Sustain. Energy Rev.* **2016**, *60*, 1470–1497. [CrossRef]
3. Nejat, P.; Jomehzadeh, F.; Taheri, M.M.; Gohari, M.; Majid, M.Z.A. A global review of energy consumption, CO_2 emissions and policy in the residential sector (with an overview of the top ten CO_2 emitting countries). *Renew. Sustain. Energy Rev.* **2015**, *43*, 843–862. [CrossRef]
4. Sikder, A.; Sikder, N. A review of advanced high performance, insensitive and thermally stable energetic materials emerging for military and space applications. *J. Hazard. Mater.* **2004**, *112*, 1–15. [CrossRef] [PubMed]
5. Gouzman, I.; Grossman, E.; Verker, R.; Atar, N.; Bolker, A.; Eliaz, N. Advances in polyimide-based materials for space appli-cations. *Adv. Mater.* **2019**, *31*, e1807738. [CrossRef]
6. Majhi, S.M.; Mirzaei, A.; Kim, H.W.; Kim, S.S.; Kim, T.W. Recent advances in energy-saving chemiresistive gas sensors: A review. *Nano Energy* **2021**, *79*, 105369. [CrossRef]
7. Zhang, H.; Shi, T.; Ma, A. Recent Advances in Design and Preparation of Polymer-Based Thermal Management Material. *Polymers* **2021**, *13*, 2797. [CrossRef] [PubMed]
8. Kaya, G.G.; Deveci, H. Synergistic effects of silica aerogels/xerogels on properties of polymer composites: A review. *J. Ind. Eng. Chem.* **2020**, *89*, 13–27. [CrossRef]
9. Peng, F.; Jiang, Y.; Feng, J.; Cai, H.; Feng, J.; Li, L. Thermally insulating, fiber-reinforced alumina–silica aerogel composites with ultra-low shrinkage up to 1500 °C. *Chem. Eng. J.* **2021**, *411*, 128402. [CrossRef]
10. Su, L.; Wang, H.; Niu, M.; Fan, X.; Ma, M.; Shi, Z.; Guo, S.-W. Ultralight, Recoverable, and High-Temperature-Resistant SiC Nanowire Aerogel. *ACS Nano* **2018**, *12*, 3103–3111. [CrossRef]
11. Yue, Y.; Liu, N.; Ma, Y.; Wang, S.; Liu, W.; Luo, C.; Zhang, H.; Cheng, F.; Rao, J.; Hu, X.; et al. Highly Self-Healable 3D Mi-crosupercapacitor with MXene-Graphene Composite Aerogel. *ACS Nano* **2018**, *12*, 4224–4232. [CrossRef]
12. Liu, J.; Zhang, H.-B.; Sun, R.; Liu, Y.; Liu, Z.; Zhou, A.; Yu, Z.-Z. Hydrophobic, Flexible, and Lightweight MXene Foams for High-Performance Electromagnetic-Interference Shielding. *Adv. Mater.* **2017**, *29*, 1702367. [CrossRef]
13. An, L.; Wang, J.; Petit, D.; Armstrong, J.; Hanson, K.; Hamilton, J.; Souza, M.; Zhao, D.; Li, C.; Liu, Y.; et al. An All-Ceramic, Anisotropic, and Flexible Aerogel Insulation Material. *Nano Lett.* **2020**, *20*, 3828–3835. [CrossRef] [PubMed]
14. Karamikamkar, S.; Naguib, H.E.; Park, C.B. Advances in precursor system for silica-based aerogel production toward improved mechanical properties, customized morphology, and multifunctionality: A review. *Adv. Colloid Interface Sci.* **2020**, *276*, 102101. [CrossRef]
15. Ahankari, S.; Paliwal, P.; Subhedar, A.; Kargarzadeh, H. Recent developments in nanocellulose-based aerogels in thermal applications: A review. *ACS Nano* **2021**, *15*, 3849–3874. [CrossRef] [PubMed]
16. Sun, Y.; Chu, Y.; Wu, W.; Xiao, H. Nanocellulose-based lightweight porous materials: A review. *Carbohydr. Polym.* **2020**, *255*, 117489. [CrossRef] [PubMed]
17. Chen, Y.; Zhang, L.; Yang, Y.; Pang, B.; Xu, W.; Duan, G.; Jiang, S.; Zhang, K. Recent progress on nanocellulose aerogels: Prepa-ration, modification, composite fabrication, applications. *Adv. Mater.* **2021**, *33*, e2005569. [CrossRef]
18. Qian, H.; Wang, J. Synthesis of lignin-poly(N-methylaniline)-reduced graphene oxide hydrogel for organic dye and lead ions removal. *J. Bioresour. Bioprod.* **2020**, *5*, 204–210. [CrossRef]
19. Shi, W.; Ching, Y.C.; Chuah, C.H. Preparation of aerogel beads and microspheres based on chitosan and cellulose for drug delivery: A review. *Int. J. Biol. Macromol.* **2021**, *170*, 751–767. [CrossRef]
20. Lin, D.; Yuen, P.Y.; Liu, Y.; Liu, W.; Liu, N.; Dauskardt, R.H.; Cui, Y. A Silica-Aerogel-Reinforced Composite Polymer Electrolyte with High Ionic Conductivity and High Modulus. *Adv. Mater.* **2018**, *30*, e1802661. [CrossRef]
21. Gao, L.; Li, C.; Huang, W.; Mei, S.; Lin, H.; Ou, Q.; Zhang, Y.; Guo, J.; Zhang, F.; Xu, S.; et al. MXene/Polymer membranes: Synthesis, properties, and emerging applications. *Chem. Mater.* **2020**, *32*, 1703–1747. [CrossRef]
22. Chen, Y.; Li, D.; Yang, W.; Xiao, C.; Wei, M. Effects of different amine-functionalized graphene on the mechanical, thermal, and tribological properties of polyimide nanocomposites synthesized by in situ polymerization. *Polymer* **2018**, *140*, 56–72. [CrossRef]
23. Li, X.; Dong, G.; Liu, Z.; Zhang, X. Polyimide Aerogel Fibers with Superior Flame Resistance, Strength, Hydrophobicity, and Flexibility Made via a Universal Sol-Gel Confined Transition Strategy. *ACS Nano* **2021**, *15*, 4759–4768. [CrossRef]

24. Wang, N.-N.; Wang, H.; Wang, Y.-Y.; Wei, Y.-H.; Si, J.-Y.; Yuen, A.C.Y.; Xie, J.-S.; Yu, B.; Zhu, S.-E.; Lu, H.-D.; et al. Robust, Lightweight, Hydrophobic, and Fire-Retarded Polyimide/MXene Aerogels for Effective Oil/Water Separation. *ACS Appl. Mater. Interfaces* **2019**, *11*, 40512–40523. [CrossRef] [PubMed]
25. Zhang, D.; Lin, Y.; Wang, W.; Li, Y.; Wu, G. Mechanically strong polyimide aerogels cross-linked with dopa-mine-functionalized carbon nanotubes for oil absorption. *Appl. Surf. Sci.* **2021**, *543*, 148833. [CrossRef]
26. Wang, D.; Peng, H.; Yu, B.; Zhou, K.; Pan, H.; Zhang, L.; Li, M.; Liu, M.; Tian, A.; Fu, S. Biomimetic structural cellulose nanofiber aerogels with exceptional mechanical, flame-retardant and thermal-insulating properties. *Chem. Eng. J.* **2020**, *389*, 124449. [CrossRef]
27. Zhu, J.; Xiong, R.; Zhao, F.; Peng, T.; Hu, J.; Xie, L.; Xie, H.; Wang, K.; Jiang, C. Lightweight, High-Strength, and Anisotropic Structure Composite Aerogel Based on Hydroxyapatite Nanocrystal and Chitosan with Thermal Insulation and Flame Retardant Properties. *ACS Sustain. Chem. Eng.* **2019**, *8*, 71–83. [CrossRef]
28. Li, Y.; Liu, X.; Nie, X.; Yang, W.; Wang, Y.; Yu, R.; Shui, J. Multifunctional organic–inorganic hybrid aerogel for self-cleaning, heat-insulating, and highly efficient microwave absorbing material. *Adv. Funct. Mater.* **2019**, *29*, 1807624. [CrossRef]
29. Zhou, Y.; Wang, S.-J.; Li, D.-S.; Jiang, L. Lightweight and recoverable ANF/rGO/PI composite aerogels for broad and high-performance microwave absorption. Compos. *Part B Eng.* **2021**, *213*, 108701. [CrossRef]
30. Feng, Y.; Wang, H.; Xu, J.; Du, X.; Cheng, X.; Du, Z.; Wang, H. Fabrication of MXene/PEI functionalized sodium alginate aerogel and its excellent adsorption behavior for Cr(VI) and Congo Red from aqueous solution. *J. Hazard. Mater.* **2021**, *416*, 125777. [CrossRef]
31. Zhang, T.; Zhao, Y.; Muhetaer, M.; Wang, K. Silver nanoparticles cross-linked polyimide aerogels with improved high tem-perature microstructure stabilities and high mechanical performances. *Microporous Mesoporous Mater.* **2020**, *297*, 110035. [CrossRef]
32. Iglesias-Mejuto, A.; García-González, C.A. 3D-printed alginate-hydroxyapatite aerogel scaffolds for bone tissue engineering. *Mater. Sci. Eng. C* **2021**, *131*, 112525. [CrossRef]
33. Zheng, W.; Zhang, X.; Zheng, Y.; Yue, Y. "Oxynitride trap" over N/S co-doped graphene-supported catalysts promoting low temperature NH3-SCR performance: Insight into the structure and mechanisms. *J. Hazard. Mater.* **2021**, *423*, 127187. [CrossRef]
34. Zhuang, Y.; Seong, J.G.; Lee, Y.M. Polyimides containing aliphatic/alicyclic segments in the main chains. *Prog. Polym. Sci.* **2019**, *92*, 35–88. [CrossRef]
35. Ma, P.; Dai, C.; Wang, H.; Li, Z.; Liu, H.; Li, W.; Yang, C. A review on high temperature resistant polyimide films: Heterocyclic structures and nanocomposites. *Compos. Commun.* **2019**, *16*, 84–93. [CrossRef]
36. He, X.; Zhang, L.; Meng, D.; Wu, J. From hydrogel to aerogel: A green fabrication of multifunctional polyimide absorbents. *Eur. Polym. J.* **2017**, *89*, 461–467. [CrossRef]
37. Ramezanzadeh, B.; Haeri, Z.; Ramezanzadeh, M. A facile route of making silica nanoparticles-covered graphene oxide nanohybrids (SiO_2-GO); fabrication of SiO_2-GO/epoxy composite coating with superior barrier and corrosion protection performance. *Chem. Eng. J.* **2016**, *303*, 511–528. [CrossRef]
38. Xu, Q.; Chang, X.; Zhu, Z.; Xu, L.; Chen, X.; Luo, L.; Liu, X.; Qin, J. Flexible pressure sensors with high pressure sensitivity and low detection limit using a unique honeycomb-designed polyimide/reduced graphene oxide composite aerogel. *RSC Adv.* **2021**, *11*, 11760–11770. [CrossRef]
39. Xue, T.; Fan, W.; Zhang, X.; Zhao, X.; Yang, F.; Liu, T. Layered double hydroxide/graphene oxide synergistically enhanced pol-yimide aerogels for thermal insulation and fire-retardancy. *Compos. Part B Eng.* **2021**, *219*, 108963. [CrossRef]
40. Li, S.; Li, C.; Song, X.; Su, B.; Mandal, B.; Prasad, B.; Gao, X.; Gao, C. Graphene quantum dots-doped thin film nanocomposite polyimide membranes with enhanced solvent resistance for solvent-resistant nanofiltration. *ACS Appl. Mater. Interfaces* **2019**, *11*, 6527–6540. [CrossRef]
41. Zhou, X.; Ding, C.; Cheng, C.; Liu, S.; Duan, G.; Xu, W.; Liu, K.; Hou, H. Mechanical and thermal properties of electrospun pol-yimide/rGO composite nanofibers via in-situ polymerization and in-situ thermal conversion. *Eur. Polym. J.* **2020**, *141*, 110083. [CrossRef]
42. Feng, H.; Fang, X.; Liu, X.; Pei, Q.; Cui, Z.-K.; Deng, S.; Gu, J.; Zhuang, Q. Reduced polyaniline decorated reduced graphene ox-ide/polyimide nanocomposite films with enhanced dielectric properties and thermostability. *Compos. Part A Appl. Sci. Manuf.* **2018**, *109*, 578–584. [CrossRef]
43. Zhang, X.; Li, W.; Song, P.; You, B.; Sun, G. Double-cross-linking strategy for preparing flexible, robust, and multifunctional polyimide aerogel. *Chem. Eng. J.* **2019**, *381*, 122784. [CrossRef]
44. Zhong, A.; Li, J.; Zhang, Y.; Zhang, F.; Wang, T.; Zhang, G.; Sun, R.; Wong, C.-P. Low temperature microwave fabrication of three-dimensional graphene/polyimide foams with flexibility strain responsivity. *Compos. Part A Appl. Sci. Manuf.* **2020**, *137*, 105995. [CrossRef]
45. Wu, Y.; Ju, D.; Wang, H.; Zhao, H.; Sun, C.; Wu, Y.; Guo, B.; Wang, Y. Modification of surface structure and mechanical properties in polyimide aerogel by low-energy proton implantation. *Surf. Coat. Technol.* **2020**, *403*, 126364. [CrossRef]
46. Hu, C.; Qi, H.; Song, J.; Zhao, G.; Yu, J.; Zhang, Y.; He, H.; Lai, J. Exploration on the tribological mechanisms of polyimide with different molecular structures in different temperatures. *Appl. Surf. Sci.* **2021**, *560*, 150051. [CrossRef]
47. Jiang, X.; Pan, W.; Xiong, Z.; Zhang, Y.; Zhao, L. Facile synthesis of layer-by-layer decorated graphene oxide based magnetic nanocomposites for β-agonists/dyes adsorption removal and bacterial inactivation in wastewater. *J. Alloys Compd.* **2021**, *870*, 159414. [CrossRef]

48. Sasikumar, B.; Bisht, S.; Arthanareeswaran, G.; Ismail, A.F.; Othman, M.H.D. Performance of polysulfone hollow fiber membranes encompassing ZIF-8, SiO^2/ZIF-8, and amine-modified SiO^2/ZIF-8 nanofillers for CO_2/CH_4 and CO_2/N_2 gas separation. *Sep. Purif. Technol.* **2021**, *264*, 118471. [CrossRef]
49. Abbas, S.S.; Rees, G.J.; Kelly, N.L.; Dancer, C.E.J.; Hanna, J.V.; McNally, T. Facile silane functionalization of graphene oxide. *Nanoscale* **2018**, *10*, 16231–16242. [CrossRef]
50. Kong, P.; Tan, H.; Lei, T.; Wang, J.; Yan, W.; Wang, R.; Waclawik, E.R.; Zheng, Z.; Li, Z. Oxygen vacancies confined in conjugated polyimide for promoted visible-light photocatalytic oxidative coupling of amines. *Appl. Catal. B Environ.* **2020**, *272*, 118964. [CrossRef]
51. Zhang, X.; Ni, X.; Li, C.; You, B.; Sun, G. Co-gel strategy for preparing hierarchically porous silica/polyimide nanocomposite aerogel with thermal insulation and flame retardancy. *J. Mater. Chem. A* **2020**, *8*, 9701–9712. [CrossRef]
52. Hassanzadeh-Aghdam, M.; Ansari, R.; Darvizeh, A. Micromechanical modeling of thermal expansion coefficients for unidirectional glass fiber-reinforced polyimide composites containing silica nanoparticles. Compos. *Part A Appl. Sci. Manuf.* **2017**, *96*, 110–121. [CrossRef]
53. Zhang, T.; Zhao, Y.; Li, X.; Ma, X.; Li, S.; Sun, M.; Liu, H.; Wang, K. Ultralight and heat-insulating mesoporous polyimide aerogels cross-linked with aminated SiO2 nanoparticles. *Microporous Mesoporous Mater.* **2021**, *319*, 111074. [CrossRef]
54. Fu, S.-Y.; Feng, X.-Q.; Lauke, B.; Mai, Y.-W. Effects of particle size, particle/matrix interface adhesion and particle loading on mechanical properties of particulate–polymer composites. *Compos. Part B Eng.* **2008**, *39*, 933–961. [CrossRef]
55. Wu, T.; Dong, J.; De France, K.J.; Li, M.; Zhao, X.; Zhang, Q. Fabrication of polyimide aerogels cross-linked by a cost-effective amine-functionalized hyperbranched polysiloxane (NH2–HBPSi). *ACS Appl. Polym. Mater.* **2020**, *2*, 3876–3885. [CrossRef]
56. Pan, C.; Liu, L.; Chen, Q.; Zhang, Q.; Guo, G. Tough, Stretchable, Compressive Novel Polymer/Graphene Oxide Nano-composite Hydrogels with Excellent Self-Healing Performance. *ACS Appl. Mater. Interfaces* **2017**, *9*, 38052–38061. [CrossRef]
57. Zou, W.; Dong, J.; Luo, Y.; Zhao, Q.; Xie, T. Dynamic covalent polymer networks: From old chemistry to modern day innovations. *Adv. Mater.* **2017**, *29*, 1606100. [CrossRef]
58. Zheng, Y.; Li, Y.; Li, Z.; Wang, Y.; Dai, K.; Zheng, G.; Liu, C.; Shen, C. The effect of filler dimensionality on the electromechanical performance of polydimethylsiloxane based conductive nanocomposites for flexible strain sensors. *Compos. Sci. Technol.* **2017**, *139*, 64–73. [CrossRef]
59. Jiang, S.; Cheong, J.Y.; Nam, J.S.; Kim, I.-D.; Agarwal, S.; Greiner, A. High-density Fibrous Polyimide Sponges with Superior Mechanical and Thermal Properties. *ACS Appl. Mater. Interfaces* **2020**, *12*, 19006–19014. [CrossRef]
60. Yang, X.; Fan, S.; Li, Y.; Guo, Y.; Li, Y.; Ruan, K.; Zhang, S.; Zhang, J.; Kong, J.; Gu, J. Synchronously improved electromagnetic interference shielding and thermal conductivity for epoxy nanocomposites by constructing 3D copper nanowires/thermally annealed graphene aerogel framework. Compos. *Part A Appl. Sci. Manuf.* **2019**, *128*, 105670.
61. Jin, X.; Wang, J.; Dai, L.; Liu, X.; Li, L.; Yang, Y.; Cao, Y.; Wang, W.; Wu, H.; Guo, S. Flame-retardant poly(vinyl alcohol)/MXene multilayered films with outstanding electromagnetic interference shielding and thermal conductive performances. *Chem. Eng. J.* **2020**, *380*, 122475. [CrossRef]
62. Zhang, Z.; Ouyang, Y.; Cheng, Y.; Chen, J.; Li, N.; Zhang, G. Size-dependent phononic thermal transport in low-dimensional nanomaterials. *Phys. Rep.* **2020**, *860*, 1–26. [CrossRef]
63. Qin, Y.; Peng, Q.; Ding, Y.; Lin, Z.; Wang, C.; Li, Y.; Xu, F.; Li, J.; Yuan, Y.; He, X.; et al. Lightweight, Superelastic, and Mechanically Flexible Graphene/Polyimide Nanocomposite Foam for Strain Sensor Application. *ACS Nano* **2015**, *9*, 8933–8941. [CrossRef] [PubMed]
64. Yao, K.; Chen, J.; Li, P.; Duan, G.; Hou, H. Robust strong electrospun polyimide composite nanofibers from a ternary polyamic acid blend. *Compos. Commun.* **2019**, *15*, 92–95. [CrossRef]
65. Wang, D.; Sun, Q.; Hokkanen, M.J.; Zhang, C.; Lin, F.-Y.; Liu, Q.; Zhu, S.-P.; Zhou, T.; Chang, Q.; He, B.; et al. Design of robust superhydrophobic surfaces. *Nature* **2020**, *582*, 55–59. [CrossRef]